THE JOURNAL OF PHYSICAL CHEMISTRY B

Article

Cite This: J. Phys. Chem. B XXXX, XXX, XXX−XXX

pubs.acs.org/JPCB

Solution Structure and Conformational Flexibility in the Active State of the Orange Carotenoid Protein. Part II: Quasielastic Neutron Scattering

Maksym Golub,[†] Marcus Moldenhauer,[‡] Franz-Josef Schmitt,[‡] Wiebke Lohstroh,[§] Eugene G. Maksimov,[∥] Thomas Friedrich,[‡] and Jörg Pieper*[,†]

[†]Institute of Physics, University of Tartu, 50411 Tartu, Estonia

[‡]Technische Universität Berlin, Institute of Chemistry, Physical Chemistry, 10623 Berlin, Germany

[§]Heinz Maier-Leibnitz Zentrum, Technische Universität München, Garching, Germany

[∥]Department of Biophysics, M. V. Lomonosov Moscow State University, Moscow, Russia

ABSTRACT: Orange carotenoid proteins (OCPs), which are protecting cyanobacterial light-harvesting antennae from photodamage, undergo a pronounced structural change upon light absorption. In addition, the active state is anticipated to boost a significantly higher molecular flexibility similar to a "molten globule" state. Here, we used quasielastic neutron scattering to directly characterize the vibrational and conformational molecular dynamics of OCP in its ground and active states, respectively, on the picosecond time scale. At a temperature of 100 K, we observe mainly (vibronic) inelastic features with peak energies at 5 and 6 meV (40 and 48 cm^{-1}, respectively). At physiological temperatures, however, two (Lorentzian) quasielastic components represent localized protein motions, that is, stochastic structural fluctuations of protein side chains between various conformational substates of the protein. Global diffusion of OCP is not observed on the given time scale. The slower Lorentzian component is affected by illumination and can be well-characterized by a jump-diffusion model. While the jump diffusion constant D is $(2.82 \pm 0.01) \times 10^{-5}$ cm^2/s at 300 K in the ground state, it is increased by ∼20% to $(3.48 \pm 0.01) \times 10^{-5}$ cm^2/s in the active state, revealing a strong enhancement of molecular mobility. The increased mobility is also reflected in the average atomic mean square displacement $\langle u^2 \rangle$; we determine a $\langle u^2 \rangle$ of 1.47 ± 0.05 Å in the ground state, but 1.86 ± 0.05 Å in the active state (at 300 K). This effect is assigned to two factors: (i) the elongated structure of the active state with two widely separated protein domains is characterized by a larger number of surface residues with a concomitantly higher degree of motional freedom and (ii) a larger number of hydration water molecules bound at the surface of the protein. We thus conclude that the active state of the orange carotenoid protein displays an enhanced conformational dynamics. The higher degree of flexibility may provide additional channels for nonradiative decay so that harmful excess energy can be more efficiently converted to heat.

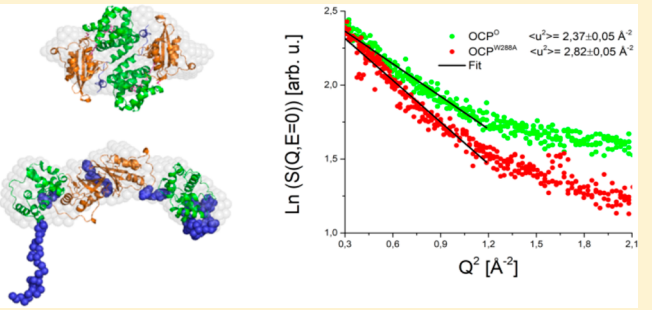

1. INTRODUCTION

Orange carotenoid proteins (OCPs) play an important role in the protection of the cyanobacterial light-harvesting apparatus against photodamage by non-photochemical quenching (NPQ) of antenna fluorescence.[1] As described in detail in the accompanying paper, OCPs undergo photoconversion from the orange ground state (OCP^O) to the active red state (OCP^R) upon absorption of blue photons (450−500 nm).[2−5] OCP is a water-soluble protein with an approximate molecular weight of ∼35 kDa and is composed of an N-terminal and a C-terminal domain (NTD and CTD, respectively) binding one xanthophyll molecule.[6,7]

The structure of the ground-state OCP^O has been known at atomic resolution for many years (see Figure 1).[8,9] Briefly, the NTD is mainly constituted by α-helices, while the CTD is composed of both α-helices and β-sheets. The two domains are interconnected by the NTD-CTD linker and by the N-terminal extension (NTE) of the NTD, that is, the αA helix attaching to a specific site on the β-sheet surface of the CTD. Furthermore, multiple protein−protein interactions across the NTD−CTD interface are stabilizing the OCP^O structure. In contrast, a high-resolution structure of the OCP^R state is not yet available, although this would be essential to understand the effective binding of OCP in its active state to the phycobilisome antennae and to the fluorescence recovery protein (FRP) as well as the underlying mechanism of photoprotection. Previous studies[6,7,10] suggest that formation of the active-state OCP^R is characterized by (i) a separation of the two domains connected

Received: May 28, 2019
Revised: August 23, 2019
Published: September 24, 2019

DOI: 10.1021/acs.jpcb.9b05073
J. Phys. Chem. B XXXX, XXX, XXX−XXX

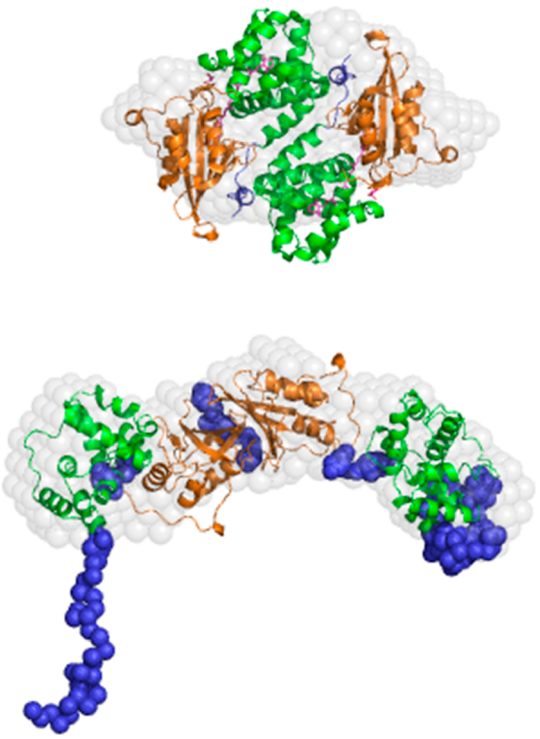

Figure 1. (top) Crystal structure of dimeric OCP^O (PDB-code 3MG1).[9] The gray spheres represent the structure of OCP reconstructed from the SANS data in the accompanying paper using the software package DAMMIF. (bottom) Structure inferred for dimeric OCP^R according to the accompanying paper.[12] The C-terminal and N-terminal domains are shown in orange and green, respectively. Flexible areas like N-terminal extension and linkers in the OCP structure are indicated in blue.

by the flexible NTD−CTD linker, (ii) a considerable increase of the protein volume along with enhanced conformational flexibility referred to as a "molten globule state",[11] and (iii) translocation of the bound carotenoid into the NTD.

In the accompanying paper,[12] we employed small-angle scattering methods combined with simulation tools to obtain solution structures of the OCP active state by in situ illumination of wild-type OCP achieving a turnover to the active state of more than 90% and by using the mutant OCP^{W288A} anticipated to mimic the active state structure. Reconstitutions of the active-state structure corroborate that OCP^R is significantly elongated compared to the ground-state OCP^O and characterized by a separation of the N-terminal and C-terminal domains with unfolded N-terminal extension (see Figure 1).

As pointed out above, the active-state OCP^R is not only characterized by a considerably altered structure but also by a specific molecular flexibility similar to a molten globule state.[10] Here, we use the definition of Ptitsyn,[11] who referred to the molten globule state as a compact intermediate with a native-like secondary structure, which is however lacking the tertiary structure of the protein's ground state. The latter situation seems to apply in the case of OCP, because CTD and NTD are well-separated, and the NTE becomes unfolded in OCP^R; see above and Figure 1.

Generally, conformational flexibility is considered as prerequisite for protein function,[13−17] especially when functional competence of proteins requires large-scale structural changes as in the case of OCP. Dynamics-function relationships are usually inferred when conformational protein motions and biological activity are simultaneously suppressed or cease below characteristic temperatures or hydration levels. For instance, specific electron transfer steps in photosynthetic reaction centers are impaired upon temperature decrease or dehydration and thus appear to require the presence of conformational protein dynamics.[18,19] In contrast, photosynthetic antenna complexes remain operative even at low temperatures, because—in terms of protein dynamics—their function mainly requires harmonic protein vibrations.[20,21]

Neutron spectroscopic methods like inelastic and quasielastic neutron scattering (INS and QENS) are powerful experimental tools for direct investigations of vibrational and conformational protein dynamics (for reviews, see refs 22−24). Because of the high incoherent scattering cross section of hydrogen atoms, which are almost homogeneously distributed in biomolecules, INS and QENS are widely used to study molecular motions in proteins. QENS experiments have shown that proteins[25−29] and biological membranes[19,30−32] display complex hydration-dependent conformational (diffusive) dynamics at physiological temperatures above a dynamical transition. The latter transition occurs in the temperature range from 200 to 240 K depending on the particular protein and on its specific environment. Hydration water dynamics can also be studied by QENS using contrast variation.[33,34] INS spectra of proteins generally display a distinct inelastic peak centered at energies of 2−7 meV representing vibrational modes of the protein (see, e.g., refs 21, 35, and 36). Furthermore, QENS data are complementary to molecular dynamics (MD) simulations of internal protein motions.[24,37−39]

It is of particular interest to this study that QENS has also established the effect of unfolding on protein dynamics,[40] which can be more generally viewed as a large-scale structural change increasing the motional degrees of freedom of protein residues at the surface along with a higher hydration due to a larger number of bound water molecules. Somewhat similar effects can be expected upon the light-induced transition from OCP^O to OCP^R; see above. In this study, we provide the first comparative characterization of protein dynamics of OCP^O and the mutant OCP^{W288A}, which can be viewed as a structural and constitutively functional analogue to OCP^R.[41]

The small-angle experiments presented in the accompanying paper reveal that the OCP^O and OCP^{W288A} samples used for QENS experiments in the present study are preferentially dimeric and widely resemble the structures of the ground and active states of OCP described above, respectively. This enables us to properly characterize the molecular dynamics of both states of OCP on the picosecond time scale. The results reveal a general enhancement of protein flexibility in the functionally active form represented by OCP^{W288A} compared to that of the structurally more compact OCP in its basal orange state OCP^O. The data can also be used as a benchmark for MD simulations and thus shed more light on the manifold of conformational substates in the active state of OCP^{W288A}.

2. MATERIALS AND METHODS

Sample Preparation. The sample preparation including cloning of cDNA and protein purification is described in detail in the accompanying paper.[12] The large amount of protein that is necessary for QENS experiments was produced by using a rich minimal medium.[42] Finally, ∼6 L of MTM was used to obtain a total of 100 mg of protein for QENS experiments. The

DOI: 10.1021/acs.jpcb.9b05073
J. Phys. Chem. B XXXX, XXX, XXX−XXX

buffer was exchanged from H_2O to D_2O to suppress the solvent scattering in the QENS experiments. This was achieved by using a phosphate buffer in D_2O prepared by dissolving a phosphate-buffered saline (PBS) tablet (Life Technologies) in 100 mL of D_2O (Sigma-Aldrich, 99.9% D content). The purified proteins were concentrated in a centrifugation concentration filter (PALL corporation Macrosep) to 400−500 μL and diluted with D_2O phosphate buffer three to four times, until a D_2O content of 99.9% was reached. The protein solutions were sealed in small tubes and frozen at −80 °C until use.

Experimental Methods. *QENS Experiments and Data Analysis.* QENS spectra were recorded using the time-of-flight spectrometer TOFTOF, operated by Technische Universität München at the Heinz Maier-Leibnitz Zentrum (MLZ) (Garching, Germany).[43] The incident neutron wavelength was 5 Å (~3.2 meV) corresponding to an (elastic) Q range of ~0.1−2.3 Å^{-1}. In this configuration, the chopper speed was 14 000 rotations per minute with a ratio of the frame-overlap chopper of 2. The typical run time for one protein sample at one temperature was 4 h. The elastic resolution of ΔE = 0.08 meV was determined by vanadium standard runs. The samples were kept in cylindrical aluminum cells having an effective volume of 1 mL. The raw neutron data were normalized to incoming flux and vanadium, corrected for the contribution of the empty cell and detector efficiency, and then transferred to energy and momentum transfer scale to obtain the scattering function $S(\mathbf{Q},\omega)$ using the program package MANTID.[44,45] OCP and OCP^{W288A} in solution as well as the D_2O-containing buffer solution were studied separately to independently investigate the contribution of the solvent at temperatures between 100 and 300 K.

In the case of a protonated scatterer like a protein, the experimental scattering function $S_{exp}(\mathbf{Q},\omega)$ can be described as (for an overview, see, e.g., ref 46)

$$S_{exp}(\mathbf{Q},\omega) = F_N \exp\left(-\frac{\hbar\omega}{2kT}\right) R(\mathbf{Q},\omega) \otimes S_{theo}(\mathbf{Q},\omega) \quad (1)$$

which is the product of a normalization factor F_N, the detailed balance factor $\exp\left(-\frac{\hbar\omega}{2kT}\right)$, and the convolution of an experimentally obtained resolution function $R(\mathbf{Q},\omega)$ with a theoretical model function $S_{theo}(\mathbf{Q},\omega)$ describing the dynamics of the sample system. The theoretical scattering function can be described by the following phenomenological model function:

$$S_{theo}(\mathbf{Q},\omega) = e^{-\langle u^2\rangle Q^2}\left\{A_0(\mathbf{Q})\delta(\omega) + \sum_n A_n(\mathbf{Q}) L_n(H_n,\omega) + S_{in}(\mathbf{Q},\omega)\right\} \quad (2)$$

Here, the scattered intensity is the product of the Debye−Waller factor $e^{-\langle u^2\rangle Q^2}$, characterized by the "global" vibrational mean square displacement $\langle u^2\rangle$ and the sum of three contributions: (i) the elastic component $A_0(Q)\delta(\omega)$, (ii) the quasielastic component $\sum_n A_n(\mathbf{Q}) L_n(H_n,\omega)$, and (iii) the inelastic contribution $S_{in}(\mathbf{Q},\omega)$ describing low-frequency vibrational motions of the protein (typically found as a band of energies in the order of a few meV). In the simplest case of an exponential protein relaxation, the line shape function $L_n(H_n,\omega)$ is a Lorentzian, whose width (H_n, half width at half-maximum (HWHM)) is related to the characteristic decay time τ_R of the relaxation process. $A_0(Q)$ and $A_n(Q)$ are the elastic and quasielastic incoherent structure factors (EISF and QISF), respectively, which are related to each other according to

$$\sum_n A_n(\mathbf{Q}) = 1 - A_0(\mathbf{Q}) \quad (3)$$

The QENS spectra were analyzed using a model-free approach. Therefore, each spectrum was fitted by a sum of an elastic Gaussian contribution identical with the resolution function and two Voigt functions representing the convolution of a Lorentzian with the Gaussian elastic peak. The HWHM of the Lorentzian curves as a function of Q^2 provides information on types of motions.[46] While Lorentzians exhibiting a constant HWHM over all Q groups are indicative of rather localized motions like, for example, a rotational diffusion, the Lorentzian HWHM of a jump diffusion follows

$$\mathrm{HWHM}(Q) = \frac{DQ^2}{1 + DQ^2\tau} \quad (4)$$

where τ represents the residence time before the jump, and D is the jump diffusion constant.

3. RESULTS AND DISCUSSION

Separation of Buffer and Protein Scattering. In a QENS experiment of a protein sample in solution, the overall scattering signal will be generally composed of contributions from both protein and solvent. This is illustrated in Figure 2, where the angle spectrum (diffractogram), that is, the scattering intensity at each angle averaged over all neutron

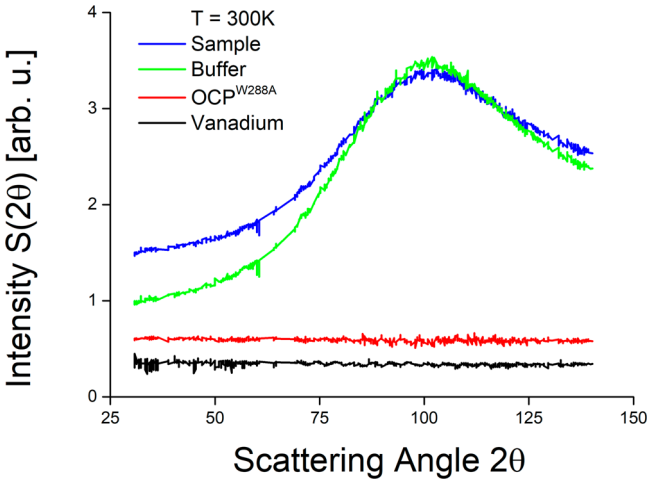

Figure 2. Buffer subtraction for the case of the OCP^{W288A} sample: Angle spectra (diffractograms) of OCP^{W288A} in buffer solution (blue line), a separate buffer sample (green line), and vanadium as an incoherent standard sample (black line) measured at 300 K. Each data point is scattering intensity at a specific angle averaged over all neutron energies; see below. The OCP^{W288A} contribution (red line) is obtained by subtraction of the buffer signal from the sample data under the condition that the coherent peak at ~100° vanishes. As a result, the OCP^{W288A} contribution is featureless as expected for an incoherent scatterering. The scaling factor to subtract the buffer is found to be 0.76.

DOI: 10.1021/acs.jpcb.9b05073
J. Phys. Chem. B XXXX, XXX, XXX−XXX

energies, of OCP^{W288A} in buffer solution (blue line) is compared with those of a separate buffer measurement (green line) and of a vanadium standard. The sample solution reveals a correlation peak at a 2θ value of ~100°. The same correlation peak is present in the buffer data so that it can be identified with the coherent scattering of D_2O. In contrast, a protein is expected to be an incoherent scatterer as the vanadium standard;[47] that is, it should display a flat background in the angle spectrum. Following,[48] the OCP^{W288A} contribution is obtained by subtraction of the buffer signal from the sample data under the condition that the coherent peak at ~100° vanishes according to

$$I_{protein} = I_{sample} - k \cdot I_{buffer} \quad (5)$$

where k is a scaling factor, which was found to be 0.76 in the case of OCP^{W288A} (and 0.81 in the case of OCP^{O}, not shown). As a result, the OCP^{W288A} contribution to the angle spectrum shown as a red line in Figure 2 is featureless confirming the validity of the approach.

Having determined the scaling factor for the solvent, the contributions of OCP^{W288A} and of the buffer solution to the QENS spectra can be reliably separated. Figure 3 shows the

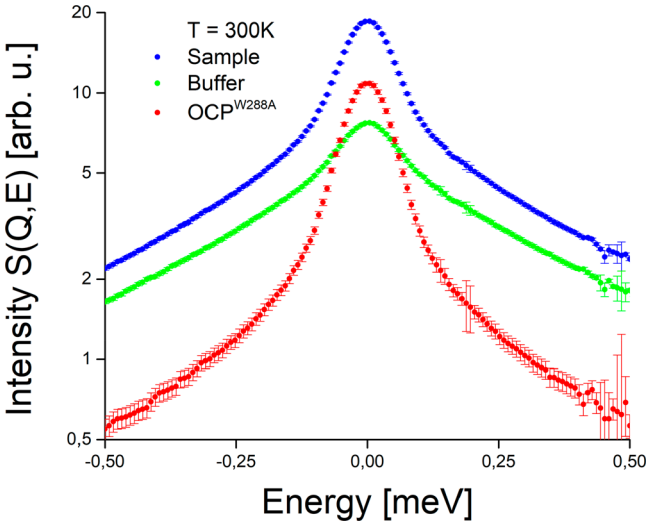

Figure 3. Buffer subtraction for the case of the OCP^{W288A} sample: QENS spectra of OCP^{W288A} in buffer solution (blue line) and of a separate buffer sample (green line) measured at 300 K and averaged over all scattering angles. The OCP^{W288A} contribution (red line) is obtained by subtraction of the buffer signal from the sample data using the scaling factor obtained in Figure 2. The color code is the same as in Figure 2.

spectra for the sample solution (blue line), separate buffer measurement (green line), as well as the difference spectrum attributed to OCP^{W288A} (red line) at 300 K. The QENS spectra displayed in Figure 3 directly correspond to the angle spectra shown in Figure 2 and show that the dynamics of OCP^{W288A} and of the buffer solution are very different. The buffer spectrum exhibits a broad quasielastic contribution, which is most likely dominated by the fast diffusion of D_2O. In comparison, the OCP^{W288A} spectrum is much narrower consistent with slower protein dynamics. It is notable that the buffer contribution accounts for a significant part of the QENS spectrum of the OCP^{W288A} sample in buffer solution and may thus largely hide the protein contribution without a reliable separation. Finally, it has to be mentioned that the difference spectrum accounts for OCP^{W288A} and its hydration shell of tightly bound water not reflected by buffer dynamics. The QENS spectrum of OCP is determined in the same way (not shown). In the following, we discuss only the QENS spectra of the protein contributions of OCP and OCP^{W288A}, respectively.

The low-temperature spectra were treated in the same way using same the scaling factors as determined at 300 K. This procedure also yielded diffractograms for OCP^{O} and OCP^{W288A} (see Figure 4) with a flat intensity distribution as expected for

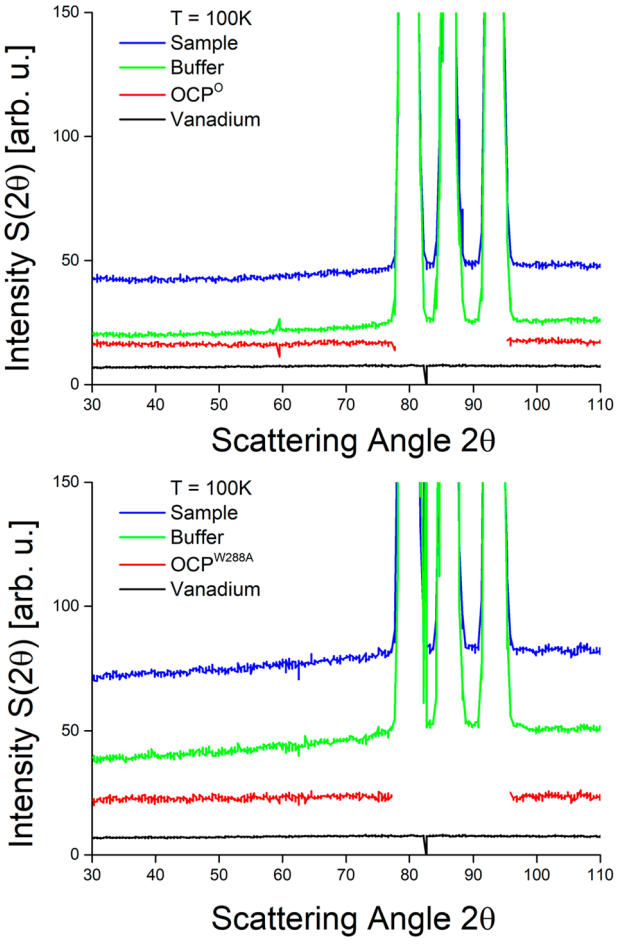

Figure 4. Buffer subtraction for the case OCP^{O} (upper) and OCP^{W288A} (lower): Angle spectra (diffractograms) of the respective sample in buffer solution (blue line), a separate buffer sample (green line), and vanadium as an incoherent standard (black line) measured at 100 K.

incoherent scatterers like proteins. The only difference to the situation at room temperature is that the buffer exhibits Bragg peaks corresponding to ice formed at 100 and 200 K, respectively. The Bragg peak region is excluded from further analysis because of improper subtraction due to high Bragg peak intensity.

Temperature Dependence of Protein Dynamics. QENS spectra of OCP^{O} and OCP^{W288A} are shown in Figure 5 for three selected temperatures aiming to characterize the temperature dependence of protein dynamics. The spectra measured at 100 and 200 K are mainly composed of an elastic peak at zero energy and a broad inelastic feature with peaks at ~5 and 6 meV (40 and 48 cm^{-1}, respectively), which can be

DOI: 10.1021/acs.jpcb.9b05073
J. Phys. Chem. B XXXX, XXX, XXX−XXX

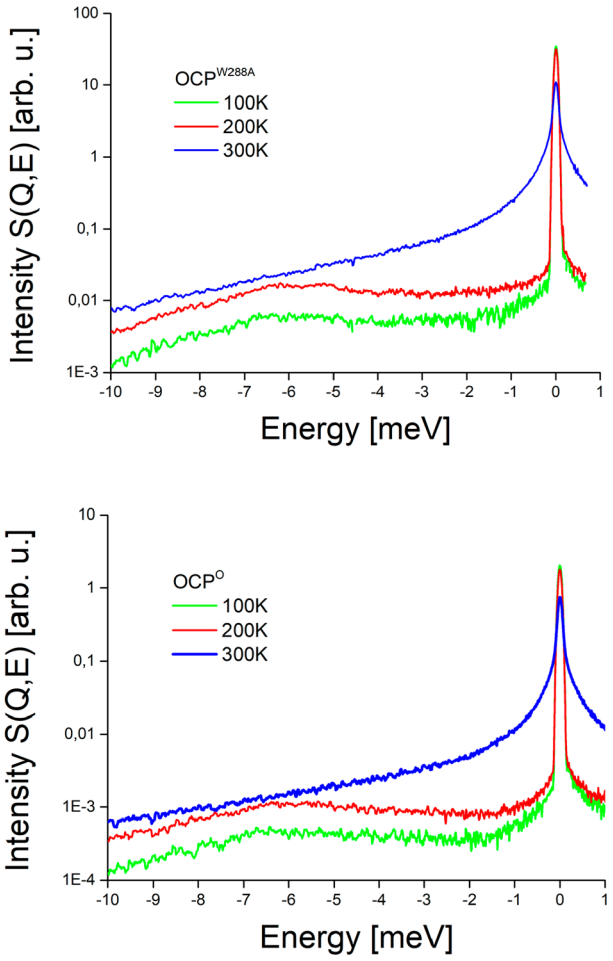

Figure 5. QENS spectra of OCP^O (lower) and OCP^{W288A} (upper) measured at different temperatures of 100 K (green line), 200 K (red line) and 300 K (blue line). The spectra are averaged over the q-range from 0.3 to 2.3 $Å^{-1}$ resulting in an average momentum transfer value of q = 1.3 $Å^{-1}$ to improve the statistics in the inelastic region.

associated with protein vibrations. The inelastic range of the QENS spectra does not reveal apparent differences between OCP^O and OCP^{W288A} at the given signal-to-noise ratio. Generally, the protein vibrations of both proteins are characterized by relatively high protein frequencies compared with other proteins typically showing vibrational peaks at ~2.5 meV.[21,35] The relatively high vibrational frequencies observed can be explained by a relatively high degree of localization of the corresponding vibrations. Similarly high vibrational frequencies were recently reported for phycobiliproteins of *A. marina*.[49] With temperature increase from 100 to 200 K, the inelastic contribution gains intensity on the expense of the elastic peak due to higher thermal occupation of vibrational levels. At the same time, the inelastic peak energies remain almost constant underlining the harmonic nature of the corresponding vibrations.

In a next step, we attempted fits of the low-temperature QENS spectra of OCP^O and OCP^{W288A} (100 and 200 K) according to eq 2 using a Gaussian function as elastic peak, a Lorentzian function (q-independent HWHM of 0.32 meV) to model a potential quasielastic contribution and an inelastic peak. At 100 K, the EISFs determined are generally well above 0.995 so that the quasielastic contribution accounts for less than 0.5% of the scattering intensity (not shown). This shows that quasielastic scattering is widely absent so that conformational motions are impaired. When the same model is applied to the QENS data measured at 200 K (see representative fit in Figure 6), some quasielastic contribution can be detected. The

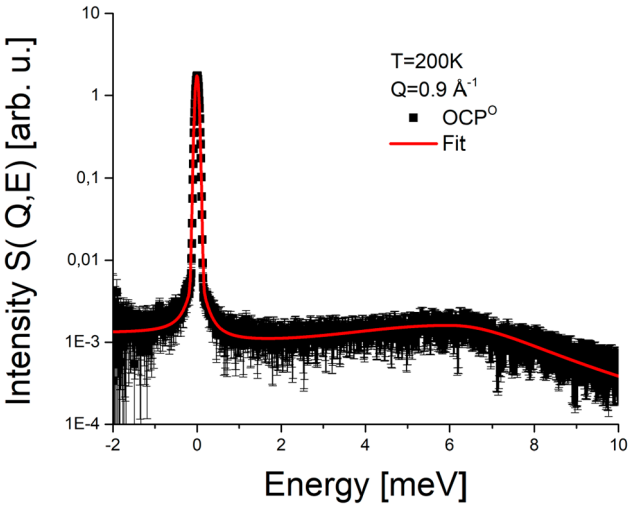

Figure 6. Representative QENS spectrum of OCP^O shown for a selected Q-value of 0.9 $Å^{-1}$ at 200 K. The full red line is a Lorentzian fit of a QENS spectrum of OCP^O; see text for details.

width (HWHM) of 0.32 meV obtained for the Lorentzian is q-independent, suggesting that the motions detected are widely localized as generally observed for proteins in this temperature region.[25] The q-dependence of the corresponding EISFs of OCP^O and OCP^{W288A} are shown in Figure 7. The EISFs are

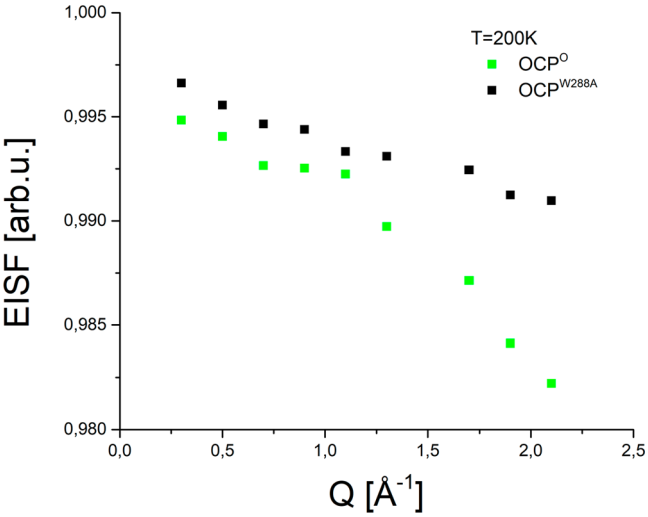

Figure 7. Comparison of the EISFs obtained from Lorentzian fits of QENS spectra of OCP^{W288A} and OCP^O, respectively, at 200 K as a function of momentum transfer Q.

generally still above 0.98 indicating that the proteins remain rather rigid at 200 K. Interestingly, however, the EISFs for OCP^O are slightly lower than those of the mutant OCP^{W288A} with separated domains and unfolded NTE. This effect could be rationalized assuming that the mutant has a larger number of surface residues whose motional freedom is hindered by the rigid (crystalline) solvent, especially the unfolded NTE. In

DOI: 10.1021/acs.jpcb.9b05073
J. Phys. Chem. B XXXX, XXX, XXX−XXX

contrast, the more compact OCP^O may retain some motional freedom in its interior.

Comparison of OCP and OCP^{W288A} Protein Dynamics at 300 K. In contrast to the situation at low temperatures, the QENS spectrum at 300 K exhibits an intense quasielastic contribution centered around the elastic peak at zero energy. This feature shows that—as an additional type of protein mobility—large-amplitude rearrangements between different conformational substates on the picosecond time scale are present at physiological temperatures. The latter type of motion is often viewed as a prerequisite for functionally important structural changes[13,14,18,50] as observed between the ground-state OCP^O and the active-state OCP^R.[51]

QENS spectra of OCP^O and OCP^{W288A} obtained at 300 K are compared in Figure 8 for a representative value of

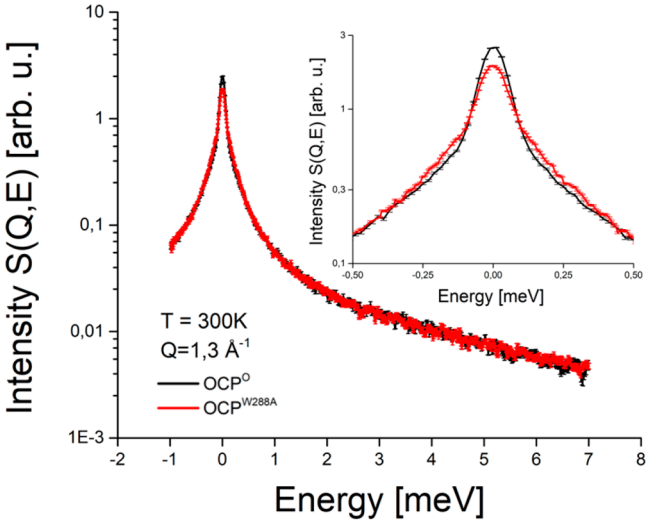

Figure 8. Comparison of QENS spectra of OCP^O (black line) and OCP^{W288A} (red line) at an average momentum transfer value of Q = 1.3 $Å^{-1}$ obtained at 300 K.

momentum transfer Q. The data reveal that OCP^{W288A} is characterized by an increased, that is, broader, quasielastic intensity in the energy range of ±0.5 meV. Qualitatively, this can be interpreted as a general increase of picosecond protein flexibility of the elongated OCP^{W288A} structure compared with OCP^O. To further analyze the latter change in conformational flexibility, the QENS spectra of OCP^O and OCP^{W288A} were fitted with phenomenological scattering functions according to eq 2. The latter fits require an elastic contribution and two Voigt functions depicting protein motions; see above. A representative fit is shown in Figure 9, and the fit parameters are compiled in Tables 1 and 2 for OCP^O and OCP^{W288A}, respectively. Here, the elastic contribution (green line in Figure 9) is determined by the resolution of the instrument. The broader of the two Lorentzians (gray line in Figure 9) characterizing faster protein motions is fixed at an HWHM of 4 meV for both OCP^O and OCP^{W288A} independent of momentum transfer Q. This is the signature expected for localized conformational protein motions of small protein residues.

A clear difference between OCP^O and OCP^{W288A} is observed for the narrow Lorentzian corresponding to slower protein motions as can also be deduced from Figure 8. The line widths (HWHM) obtained for OCP^O and OCP^{W288A} as a function of momentum transfer Q are shown in Figure 10. Obviously, the

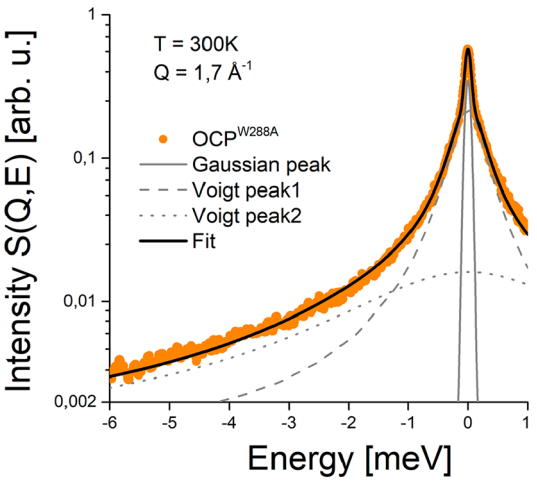

Figure 9. Example of a theoretical fit for the case of the OCP^{W288A} QENS spectrum (orange dots) at a representative momentum transfer value Q of 1.7 $Å^{-1}$. The elastic contribution is shown as a gray solid line, and the two quasielastic (Voigtian) contributions show as gray long-dashed and short-dashed lines, respectively. The final fit is shown as a black line. OCP^O data were fitted using the same model function.

line widths of OCP^{W288A} are systematically wider than those of OCP^O, which qualitatively points to a larger mobility of OCP^{W288A}. The Q-dependence can in both cases be described by a jump diffusion model (eq 4) describing localized diffusive protein motions. The mobility of the system can be quantified by a jump diffusion constant D and by the residence time τ. The full set of parameters of the fits are summarized in Table 3. According to our fits, the jump diffusion constant D found for OCP^{W288A} of (3.48 ± 0.01) × 10^{-5} cm^2/s is increased by ~20% compared to a D-value of (2.82 ± 0.01) × 10^{-5} cm^2/s derived for OCP^O. Thus, the increased D-value is a quantitative measure for a significantly enhanced protein dynamics of OCP^{W288A}, which can be viewed as a structural analogue of the active-state OCP^R. A global diffusion as observed for WSCP[48] or hemoglobin[52] could not be detected on the given time scale of motions. This is consistent with rather slow values of translational diffusion for both OCP forms observed by fluorescence correlation spectroscopy.[53]

As a further quantitative measure of the protein mobility of OCP^O and OCP^{W288A}, we determined the average atomic mean square displacement $\langle u^2 \rangle$. Briefly, Figure 11 shows the natural logarithm of the integrated intensity in the elastic peak region of OCP^O and OCP^{W288A} as a function of momentum transfer Q^2. The quasielastic contribution in the region of the elastic peak was estimated just outside of the elastic peak region and subsequently subtracted as a flat background. Both data sets exhibit linear ranges at low Q. The larger slope of the linear range for OCP^{W288A} corresponds to a larger mean square displacement $\langle u^2 \rangle$ compared with OCP^O, which again corroborates a larger mobility of OCP^{W288A}.

The observed enhanced flexibility of the signaling state analogue OCP^{W288A}—whose structure is believed to mimic that of the active-state OCP^R—can be understood in terms of the structural differences between OCP^O and OCP^{W288A}. As already discussed above, the NTD and CTD are separated in OCP^{W288A} leading to a more elongated structure of the molecule. In addition, the NTE and domain linkers are unfolded and provide additional flexibility by themselves.[54] This situation is illustrated in Figure 1 and—for the OCP^{W288A}

DOI: 10.1021/acs.jpcb.9b05073
J. Phys. Chem. B XXXX, XXX, XXX−XXX

Table 1. Parameters Used to Fit the QENS Spectra of OCP^O at 300 K

QENS fitting parameters OCP^O							
Q, Å^{-1}	area Gauss	area Lorentz1	area Lorentz2	EISF	FWHM[a] 1 meV	FWHM[a] 2 meV	Gauss width, meV
0.3	0.509 09	0.188 07	0.06	0.672 37	0.21	4	0.073
0.5	0.371 42	0.3098	0.06	0.501 09	0.21	4	0.075
0.7	0.257 32	0.4	0.105	0.337 55	0.21	4	0.075
0.9	0.218 92	0.419 17	0.11	0.292 64	0.233 66	4	0.08
1.1	0.189 57	0.411 35	0.16	0.227 94	0.307 05	4	0.082
1.3	0.193 07	0.4549	0.2	0.227 68	0.407 37	4	0.084
1.5	0.173 33	0.546 81	0.24	0.180 53	0.479 07	4	0.084
1.7	0.174 82	0.630 27	0.32	0.155 38	0.551 78	4	0.084
1.9	0.147 86	0.648 08	0.35	0.129 03	0.609 18	4	0.086
2.1	0.12	0.45	0.44	0.118 81	0.65	4	0.087

[a]FWHM = full width at half-maximum.

Table 2. Parameters Used to Fit the QENS Spectra of OCP^{W288A} at 300 K

QENS fitting parameters OCP^{W288A}							
Q, Å^{-1}	area Gauss	area Lorentz1	area Lorentz2	EISF	FWHM1 meV	FWHM2 meV	Gauss width, meV
0.3	0.241 32	0.06	0.027	0.735 01	0.19	4	0.073
0.5	0.151 51	0.110 84	0.03	0.518 25	0.19	4	0.075
0.7	0.079	0.217 66	0.042	0.233 27	0.19	4	0.075
0.9	0.071 35	0.218 77	0.047 86	0.211 11	0.278 67	4	0.08
1.1	0.053 01	0.216 24	0.062 52	0.159 78	0.346 85	4	0.082
1.3	0.050 53	0.208 13	0.072 68	0.1525	0.44	4	0.084
1.5	0.046 16	0.200 04	0.082 52	0.140 42	0.516	4	0.084
1.7	0.040 83	0.195 04	0.095	0.1234	0.567 18	4	0.084
1.9	0.031 27	0.177 34	0.12	0.095 16	0.611 82	4	0.086
2.1	0.024 91	0.175 84	0.12	0.077 66	0.669 65	4	0.087

[a]FWHM = full width at half-maximum.

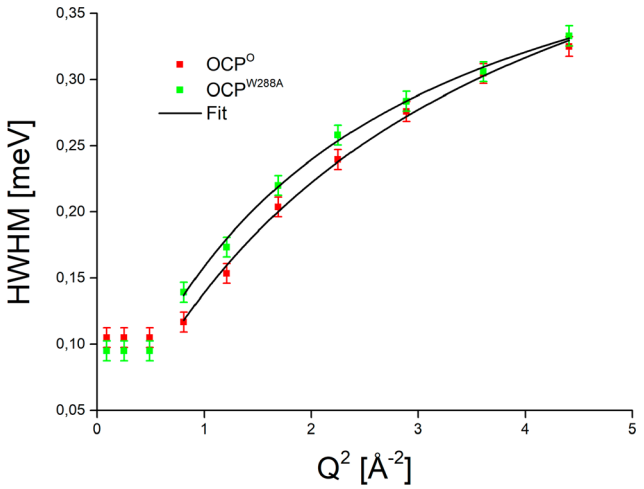

Figure 10. Q-Dependence of the HWHM of narrower quasielastic component (see gray dash line in Figure 9 for the case of OCP^{W288A}) for OCP^O and OCP^{W288A}. The lines connecting the data points are shown as a guide. The parameters of the fits are summarized in Table 3.

Table 3. Parameters of the Fits Shown in Figure 10

	OCP^O	OCP^{W288A}
jump diffusion model	narrow Lorentzian peak	
D (meV × Å^2)	0.185 ± 0.006	0.236 ± 0.006
D (10^{-5} cm^2/s)	2.82 ± 0.01	3.48 ± 0.01
t (meV^{-1})	1.81 ± 0.06	2.06 ± 0.06
t (ps)	1.18 ± 0.05	1.34 ± 0.05
constant width over all q range	broad Lorenzian peak	
HWHM (meV)	2	
t_{rot} (ps)	0.33	

sample under study here—in the inset of Figure 3. It is clearly visible that the structure of OCP^O is more compact, while OCP^{W288A} has a larger surface and some unfolded residues/linkers. In addition, under the chosen experimental settings, QENS probes the mobility of small protein residues like methyl and OH groups as well as that of water molecules on the picosecond time scale.[22−24] Taking this into account, the enhanced mobility observed for OCP^{W288A} can be attributed to two effects: (a) the larger protein surface due to separated domains and unfolded NTE leads to a higher degree of motional freedom of surface residues[40] and (b) a concomitantly higher number of hydration water molecules performing relatively fast translational and rotational motions on the protein surface themselves.[13,18,34,40] The latter dynamical component cannot be experimentally separated by our buffer subtraction approach, because the buffer dynamics is mainly determined by translational diffusion of free bulk water.[47] In contrast, the dynamics of bound hydration water molecules has been shown to be slowed compared with that of bulk water.[55] It is interesting to note that ref 56 reported a suppression of molecular dynamics upon photoactivation because of formation of additional bonds.

Protein dynamics is generally assumed to ensure functionally relevant structural changes in biomolecules.[13,14,16,18] We therefore anticipate that the enhanced flexibility directly observed by QENS for the signaling state analogue—also referred to as molten globule state—is important for the

DOI: 10.1021/acs.jpcb.9b05073
J. Phys. Chem. B XXXX, XXX, XXX−XXX

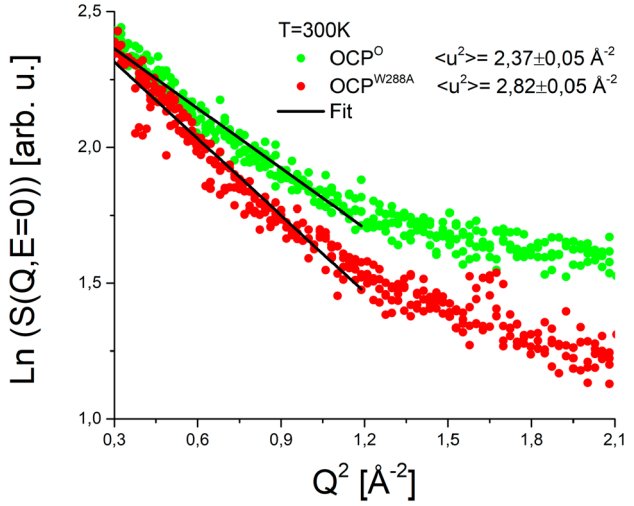

Figure 11. Determination of the average atomic mean square displacements $\langle u^2 \rangle$ of OCP^O and OCP^{W288A}: Logarithmic plot of the elastic intensities of QENS spectra as a function of momentum transfer Q^2. Linear fits of the data in the low Q-limit are shown as black lines.

function of OCP, because it may facilitate the structural changes necessary not only for binding of OCP to PBS but also for the translocation of the carotenoid in the quenching state.[54] However, there is another important aspect, as the enhanced conformational flexibility appears to be a specific property of the active state of OCP itself: the higher flexibility observed may be directly related to the reduced fluorescence quantum yield of the OCP^R-PBS complex and thus to NPQ, because excess energy can be more efficiently converted to heat by a more flexible structure due to additional channels for nonradiative decay as shown, for example, for different mutants of phytochrome[57] and cyan fluorescent proteins.[58]

4. CONCLUSIONS

In the present study, we directly investigated the picosecond molecular dynamics of OCP using quasielastic neutron scattering for the first time. We show that the jump diffusion constant D characterizing the localized stochastic fluctuations of protein residues is increased by ~20% from $(2.82 \pm 0.01) \times 10^{-5}$ cm^2/s in the ground state to $(3.48 \pm 0.01) \times 10^{-5}$ cm^2/s in the active state. At the same time, the average atomic mean square displacement $\langle u^2 \rangle$ increases from 1.47 ± 0.05 Å in the ground state to 1.86 ± 0.05 Å in the active state at 300 K. This significantly enhanced molecular mobility can be rationalized taking two factors into account: (i) the two widely separated protein domains of the active state display a larger number of surface residues along with a higher degree of motional freedom and (ii) a larger number of hydration water molecules bound at the surface of the protein. The higher degree of flexibility may provide additional channels for nonradiative decay so that harmful excess energy can be more efficiently converted to heat.

AUTHOR INFORMATION

Corresponding Author

*Phone: +(372) 737 4627. E-mail: pieper@ut.ee.

ORCID

Maksym Golub: 0000-0001-5495-9186

Jörg Pieper: 0000-0001-5995-9660

Notes

The authors declare no competing financial interest.

ACKNOWLEDGMENTS

Financial support by the Estonian Research Council (Grants PRG 539 and SLOKT 12026 T) is gratefully acknowledged. The authors also acknowledge the support of the Russian Science Foundation (Grant no. 18-44-04002), the German Ministry for Education and Research (BMBF grant no. 01DJ15007) and the German Research Foundation (DFG grant no. FR1276/5-1). F.J.S. and T.F. acknowledge financial support by Hochschulpakt Lehre III/ TU-WIMIplus program. Their work was funded by the German Research Foundation (DFG, German Research Foundation) under Germany's Excellence initiative 2005-2017 − EXC 314/1 (UniCat) and Germany's Excellence Strategy − EXC 2008/1 (UniSysCat) − 390540038. We also thank MLZ Garching for allocation of neutron beam time.

REFERENCES

(1) El Bissati, K.; Delphin, E.; Murata, N.; Etienne, A.; Kirilovsky, D. Photosystem Ii Fluorescence Quenching in the Cyanobacterium Synechocystis Pcc 6803: Involvement of Two Different Mechanisms. *Biochim. Biophys. Acta, Bioenerg.* **2000**, *1457*, 229−242.

(2) Gwizdala, M.; Wilson, A.; Kirilovsky, D. In Vitro Reconstitution of the Cyanobacterial Photoprotective Mechanism Mediated by the Orange Carotenoid Protein in Synechocystis Pcc 6803. *Plant Cell* **2011**, *23*, 2631−2643.

(3) Kirilovsky, D.; Kerfeld, C. A. The Orange Carotenoid Protein in Photoprotection of Photosystem Ii in Cyanobacteria. *Biochim. Biophys. Acta, Bioenerg.* **2012**, *1817*, 158−166.

(4) Maksimov, E. G.; Schmitt, F. J.; Shirshin, E. A.; Svirin, M. D.; Elanskaya, I. V.; Friedrich, T.; Fadeev, V. V.; Paschenko, V. Z.; Rubin, A. B. The Time Course of Non-Photochemical Quenching in Phycobilisomes of Synechocystis Sp. Pcc6803 as Revealed by Picosecond Time-Resolved Fluorimetry. *Biochim. Biophys. Acta, Bioenerg.* **2014**, *1837*, 1540−1547.

(5) Wilson, A.; Punginelli, C.; Gall, A.; Bonetti, C.; Alexandre, M.; Routaboul, J. M.; Kerfeld, C. A.; van Grondelle, R.; Robert, B.; Kennis, J. T.; et al. A Photoactive Carotenoid Protein Acting as Light Intensity Sensor. *Proc. Natl. Acad. Sci. U. S. A.* **2008**, *105*, 12075−12080.

(6) Leverenz, R. L.; Jallet, D.; Li, M. D.; Mathies, R. A.; Kirilovsky, D.; Kerfeld, C. A. Structural and Functional Modularity of the Orange Carotenoid Protein: Distinct Roles for the N- and C-Terminal Domains in Cyanobacterial Photoprotection. *Plant Cell* **2014**, *26*, 426−437.

(7) Gupta, S.; Guttman, M.; Leverenz, R. L.; Zhumadilova, K.; Pawlowski, E. G.; Petzold, C. J.; Lee, K. K.; Ralston, C. Y.; Kerfeld, C. A. Local and Global Structural Drivers for the Photoactivation of the Orange Carotenoid Protein. *Proc. Natl. Acad. Sci. U. S. A.* **2015**, *112*, 5567−5574.

(8) Kerfeld, C. A.; Sawaya, M. R.; Brahmandam, V.; Cascio, D.; Ho, K. K.; Trevithick-Sutton, C. C.; Krogmann, D. W.; Yeates, T. O. The Crystal Structure of a Cyanobacterial Water-Soluble Carotenoid Binding Protein. *Structure* **2003**, *11*, 55−65.

(9) Wilson, A.; Kinney, J. N.; Zwart, P. H.; Punginelli, C.; D'Haene, S.; Perreau, F.; Klein, M. G.; Kirilovsky, D.; Kerfeld, C. A. Structural Determinants Underlying Photoprotection in the Photoactive Orange Carotenoid Protein of Cyanobacteria. *J. Biol. Chem.* **2010**, *285*, 18364−18375.

(10) Maksimov, E. G.; Moldenhauer, M.; Shirshin, E. A.; Parshina, E. A.; Sluchanko, N. N.; Klementiev, K. E.; Tsoraev, G. V.; Tavraz, N. N.; Willoweit, M.; Schmitt, F. J.; et al. A Comparative Study of Three

DOI: 10.1021/acs.jpcb.9b05073
J. Phys. Chem. B XXXX, XXX, XXX−XXX

Signaling Forms of the Orange Carotenoid Protein. *Photosynth. Res.* **2016**, *130*, 389−401.
(11) Ptitsyn, O. B. Molten Globule and Protein Folding. *Adv. Protein Chem.* **1995**, *47*, 83−229.
(12) Golub, M.; Moldenhauer, M.; Schmitt, F. J.; Lohstroh, W.; Maksimov, E. G.; Friedrich, T.; Pieper, J. Solution Structure and Conformational Fexibility in the Active Tsate of the Orange Carotenoid Protein: Part I: Small Angle Scattering *J. Phys. Chem. B* **submitted**.
(13) Fitter, J. The Temperature Dependence of Internal Molecular Motions in Hydrated and Dry Alpha-Amylase: The Role of Hydration Water in the Dynamical Transition of Proteins. *Biophys. J.* **1999**, *76*, 1034−1042.
(14) Kühn, P.; Pieper, J.; Kaminskaya, O.; Eckert, H. J.; Lechner, R. E.; Shuvalov, V.; Renger, G. Reaction Pattern of Photosystem Ii: Oxidative Water Cleavage and Protein Flexibility. *Photosynth. Res.* **2005**, *84*, 317−323.
(15) Shlyk-Kerner, O.; Samish, I.; Kaftan, D.; Holland, N.; Sai, P. S.; Kless, H.; Scherz, A. Protein Flexibility Acclimatizes Photosynthetic Energy Conversion to the Ambient Temperature. *Nature* **2006**, *442*, 827−830.
(16) Frauenfelder, H.; Chen, G.; Berendzen, J.; Fenimore, P. W.; Jansson, H.; McMahon, B. H.; Stroe, I. R.; Swenson, J.; Young, R. D. A Unified Model of Protein Dynamic. *Proc. Natl. Acad. Sci. U. S. A.* **2009**, *106*, 5129−5134.
(17) Shlyk, O.; Samish, I.; Matenova, M.; Dulebo, A.; Polakova, H.; Kaftan, D.; Scherz, A. A Single Residue Controls Electron Transfer Gating in Photosynthetic Reaction Centers. *Sci. Rep.* **2017**, *7*, 44580.
(18) Pieper, J.; Hauss, T.; Buchsteiner, A.; Renger, G. The Effect of Hydration on Protein Flexibility in Photosystem Ii of Green Plants Studied by Quasielastic Neutron Scattering. *Eur. Biophys. J.* **2008**, *37*, 657−663.
(19) Pieper, J.; Trapp, M.; Skomorokhov, A.; Natkaniec, I.; Peters, J.; Renger, G. Temperature-Dependent Vibrational and Conformational Dynamics of Photosystem Ii Membrane Fragments from Spinach Investigated by Elastic and Inelastic Neutron Scattering. *Biochim. Biophys. Acta, Bioenerg.* **2012**, *1817*, 1213−1219.
(20) Vrandecic, K.; Rätsep, M.; Wilk, L.; Rusevich, L.; Golub, M.; Reppert, M.; Irrgang, K.-D.; Kühlbrandt, W.; Pieper, J. Protein Dynamics Tunes Excited State Positions in Light-Harvesting Complex Ii. *J. Phys. Chem. B* **2015**, *119*, 3920−3930.
(21) Golub, M.; Rusevich, L.; Irrgang, K. D.; Pieper, J. Rigid Versus Flexible Protein Matrix: Light-Harvesting Complex Ii Exhibits a Temperature-Dependent Phonon Spectral Density. *J. Phys. Chem. B* **2018**, *122*, 7111−7121.
(22) Gabel, F.; Bicout, D.; Lehnert, U.; Tehei, M.; Weik, M.; Zaccai, G. Protein Dynamics Studied by Neutron Scattering. *Q. Rev. Biophys.* **2002**, *35*, 327−367.
(23) Pieper, J.; Renger, G. Protein Dynamics Investigated by Neutron Scattering. *Photosynth. Res.* **2009**, *102*, 281−293.
(24) Vural, D.; Hu, X.; Lindner, B.; Jain, N.; Miao, Y.; Cheng, X.; Liu, Z.; Hong, L.; Smith, J. C. Quasielastic Neutron Scattering in Biology: Theory and Applications. *Biochim. Biophys. Acta, Gen. Subj.* **2017**, *1861*, 3638−3650.
(25) Roh, J. H.; Curtis, J. E.; Azzam, S.; Novikov, V. N.; Peral, I.; Chowdhuri, Z.; Gregory, R. B.; Sokolov, A. P. Influence of Hydration on the Dynamics of Lysozyme. *Biophys. J.* **2006**, *91*, 2573−2588.
(26) Doster, W.; Settles, M. Protein-Water Displacement Distributions. *Biochim. Biophys. Acta, Proteins Proteomics* **2005**, *1749*, 173−186.
(27) Matsuo, T.; Arata, T.; Oda, T.; Nakajima, K.; Ohira-Kawamura, S.; Kikuchi, T.; Fujiwara, S. Internal Dynamics of F-Actin and Myosin Subfragment-1 Studied by Quasielastic Neutron Scattering. *Biochem. Biophys. Res. Commun.* **2015**, *459*, 493−497.
(28) Fujiwara, S.; Araki, K.; Matsuo, T.; Yagi, H.; Yamada, T.; Shibata, K.; Mochizuki, H. Dynamical Behavior of Human Alpha-Synuclein Studied by Quasielastic Neutron Scattering. *PLoS One* **2016**, *11*, e0151447.
(29) Paciaroni, A.; Orecchini, A.; Cinelli, S.; et al. Protein Dynamics on the Picosecond Timescale as Affected by the Environment: A Quasielastic Neutron Scattering. *Chem. Phys.* **2003**, *292*, 397−404.
(30) Ferrand, M.; Dianoux, A. J.; Petry, W.; Zaccai, G. Thermal Motions and Function of Bacteriorhodopsin in Purple Membranes: Effects of Temperature and Hydration Studied by Neutron Scattering. *Proc. Natl. Acad. Sci. U. S. A.* **1993**, *90*, 9668−9672.
(31) Fitter, J.; Lechner, R. E.; Buldt, G.; Dencher, N. A. Internal Molecular Motions of Bacteriorhodopsin: Hydration-Induced Flexibility Studied by Quasielastic Incoherent Neutron Scattering Using Oriented Purple Membranes. *Proc. Natl. Acad. Sci. U. S. A.* **1996**, *93*, 7600−7605.
(32) Pieper, J.; Hauss, T.; Buchsteiner, A.; Baczynski, K.; Adamiak, K.; Lechner, R. E.; Renger, G. Temperature- and Hydration-Dependent Protein Dynamics in Photosystem Ii of Green Plants Studied by Quasielastic Neutron Scattering. *Biochemistry* **2007**, *46*, 11398−11409.
(33) Paciaroni, A.; Orecchini, A.; Sebastiani, F.; Sacchetti, F.; et al. Vibrational Dynamics Changes of Protein Hydration Water across the Dynamic Transition. *J. Non-Cryst. Solids* **2015**, *407*, 465−471.
(34) Schiro, G.; Fichou, Y.; Gallat, F. X.; Wood, K.; Gabel, F.; Moulin, M.; Hartlein, M.; Heyden, M.; Colletier, J. P.; Orecchini, A.; et al. Translational Diffusion of Hydration Water Correlates with Functional Motions in Folded and Intrinsically Disordered Proteins. *Nat. Commun.* **2015**, *6*, 6490.
(35) Orecchini, A.; Paciaroni, A.; Bizzarri, A. R.; Cannistraro, S. Low-Frequency Vibrational Anomalies in Beta-Lactoglobulin: Contribution of Different Hydrogen Classes Revealed by Inelastic Neutron Scattering. *J. Phys. Chem. B* **2001**, *105*, 12150−12156.
(36) Pieper, J.; Irrgang, K. D.; Renger, G.; Lechner, R. E. Density of Vibrational States of the Light-Harvesting Complex Ii of Green Plants Studied by Inelastic Neutron Scattering. *J. Phys. Chem. B* **2004**, *108*, 10556−10565.
(37) Tarek, M.; Tobias, D. J. Role of Protein-Water Hydrogen Bond Dynamics in the Protein Dynamical Transition. *Phys. Rev. Lett.* **2002**, *88*, 1−4.
(38) Kneller, G. R. Quasielastic Neutron Scattering and Relaxation Processes in Proteins: Analytical and Simulation-Based Models. *Phys. Chem. Chem. Phys.* **2005**, *7*, 2641−2655.
(39) Aoun, B.; Pellegrini, E.; Trapp, M.; Natali, F.; Cantu, L.; Brocca, P.; Gerelli, Y.; Deme, B.; Marek Koza, M.; Johnson, M.; et al. Direct Comparison of Elastic Incoherent Neutron Scattering Experiments with Molecular Dynamics Simulations of Dmpc Phase Transitions. *Eur. Phys. J. E: Soft Matter Biol. Phys.* **2016**, *39*, 48.
(40) Gallat, F. X.; Laganowsky, A.; Wood, K.; Gabel, F.; van Eijck, L.; Wuttke, J.; Moulin, M.; Hartlein, M.; Eisenberg, D.; Colletier, J. P.; et al. Dynamical Coupling of Intrinsically Disordered Proteins and Their Hydration Water: Comparison with Folded Soluble and Membrane Proteins. *Biophys. J.* **2012**, *103*, 129−136.
(41) Sluchanko, N. N.; Klementiev, K. E.; Shirshin, E. A.; Tsoraev, G. V.; Friedrich, T.; Maksimov, E. G. The Purple Trp288ala Mutant of Synechocystis Ocp Persistently Quenches Phycobilisome Fluorescence and Tightly Interacts with Frp. *Biochim. Biophys. Acta, Bioenerg.* **2017**, *1858*, 1−11.
(42) Tyler, R. C.; Sreenath, H. K.; Singh, S.; Aceti, D. J.; Bingman, C. A.; Markley, J. L.; Fox, B. G. Auto-Induction Medium for the Production of [U-15n]- and [U-13c, U-15n]-Labeled Proteins for Nmr Screening and Structure Determination. *Protein Expression Purif.* **2005**, *40*, 268−278.
(43) Lohstroh, W.; Evenson, Z. Toftof: Cold Neutron Time-of-Flight Spectrometer. *J. Large-Scale Res. Facil.* **2015**, *1*, 1−3.
(44) Arnold, O.; Bilheux, J. C.; Borreguero, J. M.; Buts, A.; Campbell, S. I.; Chapon, L.; Doucet, M.; Draper, N.; Leal, R. F.; Gigg, M. A.; et al. Mantid-Data Analysis and Visualization Package for Neutron Scattering and Mu Sr Experiments. *Nucl. Instrum. Methods Phys. Res., Sect. A* **2014**, *764*, 156−166.
(45) Manipulation and Analysis Toolkit for Instrument Data. http://dx.doi.org/10.5286/SOFTWARE/MANTID (accessed Oct 10, 2017).

DOI: 10.1021/acs.jpcb.9b05073
J. Phys. Chem. B XXXX, XXX, XXX−XXX

(46) Bee, M. *Quasielastic Neutron Scattering: Principles and Applications in Solid State Chemistry, Biological Materilas Science;* CRC Press, 1988.
(47) Gaspar, A. M.; Appavou, M. S.; Busch, S.; Unruh, T.; Doster, W. Dynamics of Well-Folded and Aatively Disordered Proteins in Solution: A Time-of-Flight Neutron Scattering Study. *Eur. Biophys. J.* **2008**, *37*, 573−582.
(48) Rusevich, L.; Embs, J.; Bektas, I.; Paulsen, H.; Renger, G.; Pieper, J. Protein and Solvent Dynamics of the Water-Soluble Chlorophyll-Binding Protein (Wscp). *EPJ Web Conf.* **2015**, *83*, 1−4.
(49) Pieper, J.; Ratsep, M.; Golub, M.; Schmitt, F. J.; Artene, P.; Eckert, H. J. Excitation Energy Transfer in Phycobiliproteins of the Cyanobacterium Acaryochloris Marina Investigated by Spectral Hole Burning. *Photosynth. Res.* **2017**, *133*, 225−234.
(50) Frauenfelder, H.; Mezei, F. Neutron Scattering and Protein Dynamics. *Acta Crystallogr., Sect. D: Biol. Crystallogr.* **2010**, *66*, 1229−1231.
(51) Maksimov, E. G.; Klementiev, K. E.; Shirshin, E. A.; Tsoraev, G. V.; Elanskaya, I. V.; Paschenko, V. Z. Features of Temporal Behavior of Fluorescence Recovery in Synechocystis Sp. Pcc6803. *Photosynth. Res.* **2015**, *125*, 167−178.
(52) Stadler, A. M.; Embs, J. P.; Digel, I.; Artmann, G. M.; Unruh, T.; Buldt, G.; Zaccai, G. Cytoplasmic Water and Hydration Layer Dynamics in Human Red Blood Cells. *J. Am. Chem. Soc.* **2008**, *130*, 16852−16853.
(53) Moldenhauer, M.; Sluchanko, N. N.; Tavraz, N. N.; Junghans, C.; Buhrke, D.; Willoweit, M.; Chiappisi, L.; Schmitt, F. J.; Vukojevic, V.; Shirshin, E. A.; et al. Interaction of the Signaling State Analog and the Apoprotein Form of the Orange Carotenoid Protein with the Fluorescence Recovery Protein. *Photosynth. Res.* **2018**, *135*, 125−139.
(54) Maksimov, E. G.; Sluchanko, N. N.; Slonimskiy, Y. B.; Mironov, K. S.; Klementiev, K. E.; Moldenhauer, M.; Friedrich, T.; Los, D. A.; Paschenko, V. Z.; Rubin, A. B. The Unique Protein-to-Protein Carotenoid Transfer Mechanism. *Biophys. J.* **2017**, *113*, 402−414.
(55) Bellissent-Funel, M. C.; Teixeira, J.; Bradley, K.; Chen, S. Dynamics of Hydration Water in Protein. *J. Phys. I* **1992**, *2*, 995−1001.
(56) Stadler, A. M.; Knieps-Grunhagen, E.; Bocola, M.; Lohstroh, W.; Zamponi, M.; Krauss, U. Photoactivation Reduces Side-Chain Dynamics of a Lov Photoreceptor. *Biophys. J.* **2016**, *110*, 1064−1074.
(57) Escobar, L. B.; Guedes, G. P.; Soriano, S.; Speziali, N. L.; Jordao, A. K.; Cunha, A. C.; Ferreira, V. F.; Maxim, C.; Novak, M. A.; Andruh, M.; et al. New Families of Hetero-Tri-Spin 2p-3d-4f Complexes: Synthesis, Crystal Structures, and Magnetic Properties. *Inorg. Chem.* **2014**, *53*, 7508−7517.
(58) Lelimousin, M.; Noirclerc-Savoye, M.; Lazareno-Saez, C.; Paetzold, B.; Le Vot, S.; Chazal, R.; Macheboeuf, P.; Field, M. J.; Bourgeois, D.; Royant, A. Intrinsic Dynamics in Ecfp and Cerulean Control Fluorescence Quantum Yield. *Biochemistry* **2009**, *48*, 10038−10046.

DOI: 10.1021/acs.jpcb.9b05073
J. Phys. Chem. B XXXX, XXX, XXX−XXX